

# Surface-Tension Replica-Exchange Molecular Dynamics Method for Enhanced Sampling of Biological Membrane Systems

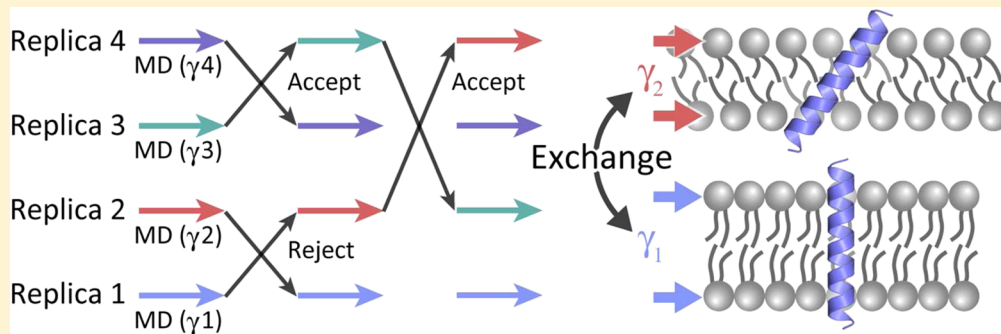
Takaharu Mori,<sup>†,‡</sup> Jaewoon Jung,<sup>§</sup> and Yuji Sugita\*,<sup>†,‡,§</sup>

<sup>†</sup>RIKEN Quantitative Biology Center, 7-1-26 minatojima-minamimachi, Chuo-ku, Kobe, Hyogo 650-0047, Japan

<sup>‡</sup>RIKEN Theoretical Molecular Science Laboratory, 2-1 Hirosawa, Wako-shi, Saitama 351-0198, Japan

<sup>§</sup>RIKEN Advanced Institute for Computational Science, 7-1-26 minatojima-minamimachi, Chuo-ku, Kobe, Hyogo 650-0047, Japan

 Supporting Information



**ABSTRACT:** Conformational sampling is fundamentally important for simulating complex biomolecular systems. The generalized-ensemble algorithm, especially the temperature replica-exchange molecular dynamics method (T-REMD), is one of the most powerful methods to explore structures of biomolecules such as proteins, nucleic acids, carbohydrates, and also of lipid membranes. T-REMD simulations have focused on soluble proteins rather than membrane proteins or lipid bilayers, because explicit membranes do not keep their structural integrity at high temperature. Here, we propose a new generalized-ensemble algorithm for membrane systems, which we call the surface-tension REMD method. Each replica is simulated in the  $N\gamma T$  ensemble, and surface tensions in a pair of replicas are exchanged at certain intervals to enhance conformational sampling of the target membrane system. We test the method on two biological membrane systems: a fully hydrated DPPC (1,2-dipalmitoyl-sn-glycero-3-phosphatidylcholine) lipid bilayer and a WALP23-POPC (1-palmitoyl-2-oleoyl-sn-glycero-3-phosphocholine) membrane system. During these simulations, a random walk in surface tension space is realized. Large-scale lateral deformation (shrinking and stretching) of the membranes takes place in all of the replicas without collapse of the lipid bilayer structure. There is accelerated lateral diffusion of DPPC lipid molecules compared with conventional MD simulation, and a much wider range of tilt angle of the WALP23 peptide is sampled due to large deformation of the POPC lipid bilayer and through peptide-lipid interactions. Our method could be applicable to a wide variety of biological membrane systems.

## I. INTRODUCTION

Biological membranes consist of lipid molecules including cholesterol as well as membrane proteins. Various cellular processes like substrate transport, signal transduction, membrane fusion, and cell adhesion occur at membrane interfaces. Membrane proteins play important roles in these processes, usually undergoing conformational changes. For example, ion channels facilitate the passage of ions across membranes by changing conformation from closed to open states.<sup>1</sup> Similarly, ion pumps, according to E1/E2 theory, change affinity for ions by assuming different conformational states, thereby transferring ions against a large concentration gradient across the membrane.<sup>2</sup> Advances in structural biology have revealed the close relationship between function and conformational changes of membrane proteins, which in many cases are now understood at atomic resolution.<sup>3</sup> Protein–lipid interactions also affect the function and conformational stability of membrane proteins,<sup>4,5</sup>

and in some cases, proteins may be located in specialized cholesterol-rich microdomains in the membrane (lipid rafts), influencing a number of cellular processes.<sup>6,7</sup> Thus, it is important to investigate how membrane proteins undergo conformational changes in realistic membrane environments.

Molecular dynamics (MD) simulation is a powerful tool to simulate the dynamics of complex biomolecular systems including biological membranes. Recent development of massively parallel supercomputers<sup>8</sup> or special purpose machines for MD simulations of biomolecules like Anton<sup>9</sup> has allowed simulation of large conformational changes of membrane proteins on time scales of tens or hundreds of microseconds.<sup>10–12</sup> However, for slow biological phenomena, it is more useful to employ efficient conformational sampling schemes in MD simulations on these

Received: May 29, 2013

Published: November 14, 2013



ACS Publications

© 2013 American Chemical Society

fast supercomputers.<sup>13,14</sup> For simulations of biological membrane systems, biased MD simulations like steered MD<sup>15,16</sup> and targeted MD methods,<sup>17</sup> and MD simulations with coarse-grained models<sup>18–20</sup> and membrane mimetic model<sup>21</sup> have been performed.

The generalized-ensemble algorithm is one of the enhanced conformational sampling methods used for systems with rugged free-energy landscapes.<sup>22–25</sup> Replica-exchange molecular-dynamics method (REMD), especially the original temperature-exchange method (T-REMD), is the most widely used in simulations of biomolecules.<sup>26,27</sup> Here, replicas (or copies) of the original system are prepared, and different temperatures are assigned to each replica. Each replica is run in a canonical (*NVT*)<sup>26</sup> or isobaric–isothermal (*NPT*) ensemble,<sup>28–30</sup> and target temperatures are exchanged between a pair of replicas during a simulation. Exchanging temperature enforces a random walk in temperature space, resulting in the simulation surmounting energy barriers and the sampling of a much wider conformational space of target molecules. The T-REMD method is applicable not only to soluble proteins but also to biological membrane systems.<sup>31,32</sup> However, T-REMD simulation of membrane systems needs to be carefully managed, because an explicit lipid bilayer does not maintain structural integrity at high temperature. Accordingly, positional restraints on the lipid bilayer are often imposed,<sup>33</sup> but these reduce the fluidity of the membrane. In other approaches, membrane proteins are simulated using the atomistic model, where membrane effects are incorporated implicitly, using the implicit model of membranes.<sup>34–37</sup>

Here, we propose a new generalized-ensemble algorithm for explicit membrane systems, which we call the surface-tension REMD method. In this method, we employ the *NPγT* ensemble<sup>38</sup> for each replica, and target surface tensions are exchanged between a pair of replicas during simulation. Surface tension is a force existing at liquid interfaces such as in vacuum/water, oil/water, and membrane/water systems. In the case of a lipid-bilayer/water system, the surface tension is zero when the bilayer is ideally flat.<sup>39,40</sup> Positive surface tension increases the surface area of a lipid bilayer and accelerates lateral diffusion of each lipid molecule, while the bilayer thickness decreases due to volume incompressibility.<sup>41–43</sup> Accordingly, the surface-tension REMD method promises to efficiently enhance the dynamics of simulated biological membrane systems without exchanging temperature.

In this study, we provide the formulation for the surface-tension REMD method, and test it on two biological membrane systems: 162 DPPC (1,2-dipalmitoyl-*sn*-glycero-3-phosphatidylcholine) lipid bilayer and WALP23–POPC (1-palmitoyl-2-oleoyl-*sn*-glycero-3-phosphocholine) membrane systems. We also compare the results of the surface-tension REMD with those of conventional MD simulation in *NPT* and *NPγT* ensembles. Finally, we discuss applicability of our method to other biological membrane systems.

## II. METHODS

**A. Theory of the *NPγT* Ensemble.** In the *NPγT* ensemble, normal pressure  $P$ , surface tension  $\gamma$ , and temperature  $T$  are kept constant during a simulation.<sup>38</sup> We consider the shape of a simulation box orthorhombic with sides of length  $h_x$ ,  $h_y$ , and  $h_z$  and a lipid bilayer parallel to the  $xy$  plane. Surface tension of the system is defined as

$$\gamma = h_z \times \left( P_{zz} - \frac{P_{xx} + P_{yy}}{2} \right) \quad (1)$$

where  $P_{zz}$  is normal pressure and  $P_{xx}$  and  $P_{yy}$  are tangential components of the pressure tensor.

We consider a system consisting of  $N$  atoms with their coordinate vectors, momentum vectors, and cell dimensions denoted by  $q = \{q_1, \dots, q_N\}$ ,  $p = \{p_1, \dots, p_N\}$ , and  $h = \{h_x, h_y, h_z\}$ , respectively. In the *NPγT* ensemble, the probability of finding the system in the state  $x = (q, p, h)$  is given by the following distribution function:

$$f(x) = C \exp[-\beta\{K(p) + E(q, h) + Ph_x h_y h_z - \gamma h_x h_y\}] \quad (2)$$

where  $C$  is a normalization constant,  $K$  is the kinetic energy given by  $K(p) = \sum_{i=1}^N (\mathbf{p}_i^2 / 2m_i)$ ,  $E$  is the potential energy, and  $\beta$  is the inverse temperature defined by  $\beta = 1/k_B T$  ( $k_B$  is the Boltzmann constant).

**B. Surface-Tension Replica-Exchange Method.** There are three exchangeable parameters for REMD in the *NPγT* ensemble: temperature, normal pressure, and surface tension. If we focus on the surface tension, it can be exchanged simultaneously with temperature ( $\gamma$ T-REMD), normal pressure ( $\gamma P$ -REMD), both of them ( $\gamma PT$ -REMD), or neither of them ( $\gamma$ -REMD). Together these methods are called “surface-tension REMD method”. Here, we derive a general formulation of the surface-tension REMD method, and also for the simplest case, namely the  $\gamma$ -REMD method.

The generalized ensemble for the replica-exchange method consists of  $M$  noninteracting replicas of the original system in the *NPγT* ensemble at  $M$  different parameter sets of normal pressure  $P$ , surface tension  $\gamma$ , and temperature  $T$ . Here, replicas are specified using labels  $i$  ( $i = 1, \dots, M$ ), and parameter sets are defined with  $\Lambda_m = (P_m, \gamma_m, T_m)$  ( $m = 1, \dots, M$ ). We arrange the replicas so that there is a one-to-one correspondence between replicas and parameter set values; the label  $i$  ( $i = 1, \dots, M$ ) for replicas is a permutation of  $m$  ( $m = 1, \dots, M$ ) for parameter sets  $\Lambda_m$ , and vice versa,

$$\begin{cases} i = i(m) \equiv \sigma(m) \\ m = m(i) \equiv \sigma^{-1}(i) \end{cases} \quad (3)$$

where  $\sigma(m)$  is a permutation function of  $m$  and  $\sigma^{-1}(i)$  is its inverse.

We define a “state” in this generalized ensemble as  $X = \{x_1^{[i(1)]}, \dots, x_M^{[i(M)]}\} = \{x_{m(1)}^{[1]}, \dots, x_{m(M)}^{[M]}\}$ , where the superscript  $i$  and subscript  $m$  in  $x_m^{[i]}$  stand for the replica index and the parameter set index, respectively. The state  $X$  is specified by the  $M$  sets of coordinates  $q^{[i]}$ , momenta  $p^{[i]}$ , and cell dimensions  $h^{[i]}$  in replica  $i$  at  $\Lambda_m = (P_m, \gamma_m, T_m)$ :

$$x_m^{[i]} = (q^{[i]}, p^{[i]}, h^{[i]})_m \quad (4)$$

Consider exchanging a pair of replicas in the generalized ensemble. Suppose we exchange replica  $i$  and  $j$  which are at  $\Lambda_m$  and  $\Lambda_n$ , respectively,

$$X = \{\dots, x_m^{[i]}, \dots, x_n^{[j]}, \dots\} \rightarrow X' = \{\dots, x_m^{[j]}, \dots, x_n^{[i]}, \dots\} \quad (5)$$

where  $x_m^{[j]}$  and  $x_n^{[i]}$  are defined with

$$\begin{cases} x_m^{[j]'} = (q^{[j]}, p^{[j]}, h^{[j]})_m \\ x_n^{[i]'} = (q^{[i]}, p^{[i]}, h^{[i]})_n \end{cases} \quad (6)$$

respectively. The momenta are rescaled as follows:

$$p^{[i]'} = \sqrt{\frac{T_n}{T_m}} p^{[i]} \quad p^{[j]'} = \sqrt{\frac{T_m}{T_n}} p^{[j]} \quad (7)$$

For this exchange process to converge toward an equilibrium distribution, it is sufficient to impose the detailed balance condition on the transition probability  $w(X \rightarrow X')$ :

$$P(X) w(X \rightarrow X') = P(X') w(X' \rightarrow X) \quad (8)$$

where  $P(X)$  is the probability of finding the system in a state  $X$  of the generalized ensemble. Because replicas are noninteracting,  $P(X)$  is given by a product of the distribution functions for each replica  $i$ ,

$$P(X) = \prod_{i=1}^M f(x_{m(i)}^{[i]}) = \prod_{m=1}^M f(x_m^{[i(m)]}) \quad (9)$$

where  $i(m)$  and  $m(i)$  are the permutation functions in eq 3. The transition probability for the replica exchange process is given by the usual Metropolis criterion,

$$w(X \rightarrow X') = \min\left(1, \frac{P(X')}{P(X)}\right) = \min(1, \exp(-\Delta)) \quad (10)$$

where we have

$$\begin{aligned} \Delta = & (\beta_m - \beta_n)\{E(q^{[j]}, h^{[j]}) - E(q^{[i]}, h^{[i]})\} \\ & + (\beta_m P_m - \beta_n P_n)(h_x^{[j]} h_y^{[j]} h_z^{[j]} - h_x^{[i]} h_y^{[i]} h_z^{[i]}) \\ & - (\beta_m \gamma_m - \beta_n \gamma_n)(h_x^{[j]} h_y^{[j]} - h_x^{[i]} h_y^{[i]}) \end{aligned} \quad (11)$$

As in the T-REMD method,<sup>26</sup> the kinetic energy terms have canceled each other out in eq 11 via rescaling of momenta by eq 7.

The transition probability (eqs 10 and 11) should be independent of constant temperature and constant pressure algorithms, whereas the momenta-rescaling scheme depends on the algorithm used in the simulation. As pointed out previously,<sup>30,44</sup> if thermostat and barostat momenta are included in the equations of motion like the Martyna–Tobias–Klein algorithm,<sup>45</sup> these variables should also be rescaled after replica exchange. In the Appendix, we present the derivations of eq 11 and rescaling scheme in the case of the Langevin dynamics method.<sup>46,47</sup>

Surface-tension REMD is realized by alternatively performing the following steps:

- (1) For each replica, MD simulation in the  $NP\gamma T$  ensemble is carried out simultaneously and independently for certain steps.
- (2) We exchange a pair of replicas  $i$  and  $j$  which are at  $\Lambda_m$  and  $\Lambda_n$ , respectively. The transition probability for this replica exchange process is given by eq 11.

In the  $\gamma$ -REMD method, only surface tensions are exchanged between replicas. In the case that all replicas have the same temperature and normal pressure values, we use the following formula for the Metropolis criterion:

$$\Delta = -\beta(\gamma_m - \gamma_n)(h_x^{[j]} h_y^{[j]} - h_x^{[i]} h_y^{[i]}) \quad (12)$$

and rescaling of momenta is not necessary according to eqs A9–A11 in the Appendix.

**C. Reweighting Techniques.** The results from a surface-tension REMD simulation can be analyzed by reweighting techniques. Here, we use the weighted histogram analysis method (WHAM).<sup>48,49</sup> Suppose that we have carried out a REMD simulation with  $M$  replicas at a condition of  $\Lambda_m$  ( $m = 1, \dots, M$ ). The expectation value of a physical quantity  $Q$  at any normal pressure  $P$ , surface tension  $\gamma$ , and temperature  $T$  is given by

$$\langle Q \rangle_{P,\gamma,T} = \frac{\sum_E \sum_V \sum_A Q(E, V, A) P_{P,\gamma,T}(E, V, A)}{\sum_E \sum_V \sum_A P_{P,\gamma,T}(E, V, A)}, \quad (13)$$

where  $P_{P,\gamma,T}(E, V, A)$  is the probability distribution at any normal pressure  $P$ , surface tension  $\gamma$ , and temperature  $T$  defined by

$$P_{P,\gamma,T}(E, V, A) = \frac{\sum_{m=1}^M g_m^{-1} N_m(E, V, A) \exp[-\beta(E + PV - \gamma A)]}{\sum_{m=1}^M g_m^{-1} n_m \exp[f_m - \beta_m(E + P_m V - \gamma_m A)]} \quad (14)$$

$$\exp(-f_m) = \sum_E \sum_V \sum_A P_{P,\gamma,T}(E, V, A) \quad (15)$$

Here,  $g_m = 1 + 2\tau_m$  and  $\tau_m$  is the integrated autocorrelation time, which can be set to a constant value for all  $m$ .<sup>49</sup>  $N_m(E, V, A)$  is the histogram of potential energy  $E$ , volume  $V$ , and area  $A$ , and  $n_m$  is the number of the data at  $\Lambda_m$ . Equations 14 and 15 are solved self-consistently by iteration.

The potential of mean force  $W$  (free energy as a function of a reaction coordinate  $\xi$ ) of the system at any normal pressure  $P$ , surface tension  $\gamma$ , and temperature  $T$  is given by

$$W_{P,\gamma,T}(\xi) = -k_B T \ln P_{P,\gamma,T}(\xi) \quad (16)$$

where the probability distribution  $P_{P,\gamma,T}(\xi)$  is obtained by solving the following WHAM equations:

$$P_{P,\gamma,T}(\xi) = \sum_E \sum_V \sum_A \frac{\sum_{m=1}^M g_m^{-1} N_m(E, V, A, \xi) \exp[-\beta(E + PV - \gamma A)]}{\sum_{m=1}^M g_m^{-1} n_m \exp[f_m - \beta_m(E + P_m V - \gamma_m A)]} \quad (17)$$

$$\exp(-f_m) = \sum_{\xi} P_{P,\gamma,T}(\xi) \quad (18)$$

$N_m(E, V, A, \xi)$  is the histogram of potential energy, volume, area, and reaction coordinates at  $\Lambda_m$ . Equations 17 and 18 are solved self-consistently by iteration.

**D. Simulation of 162 DPPC System.** The initial structure of a 162 DPPC lipid bilayer was modeled by utilizing the CHARMM-GUI membrane builder.<sup>50</sup> The system contained 162 DPPC lipid molecules and 9207 TIP3P waters (total 48 681 atoms), where the initial box size was  $(h_x, h_y, h_z) = (69.48 \text{ \AA}, 69.48 \text{ \AA}, 107.24 \text{ \AA})$ . We gradually equilibrated the system in multiple steps, first a 20 000 step energy minimization, followed by 31 ns equilibration. For the first 1 ns, MD simulation in the *NVT* ensemble ( $T = 323.15 \text{ K}$ ) was carried out with positional restraints on the lipid head groups. We then performed a 4 ns MD simulation in the *NPAT* ensemble<sup>38</sup> ( $P = 1 \text{ atm}$ ,  $T = 323.15 \text{ K}$ , and  $A = h_x \times h_y$ ) with positional restraints on the direction of lipid head groups normal to the bilayer, and these restraints were gradually reduced to zero. An 11 ns MD simulation was then carried out in the *NPT* ensemble ( $P = 1 \text{ atm}$  and  $T = 323.15 \text{ K}$ ) without any restraints on the system. Finally, to prepare the initial structure of each replica in the  $\gamma$ -REMD simulation, we performed MD simulations for 15 ns in the *NP*/ $\gamma$  ensemble.<sup>38</sup>

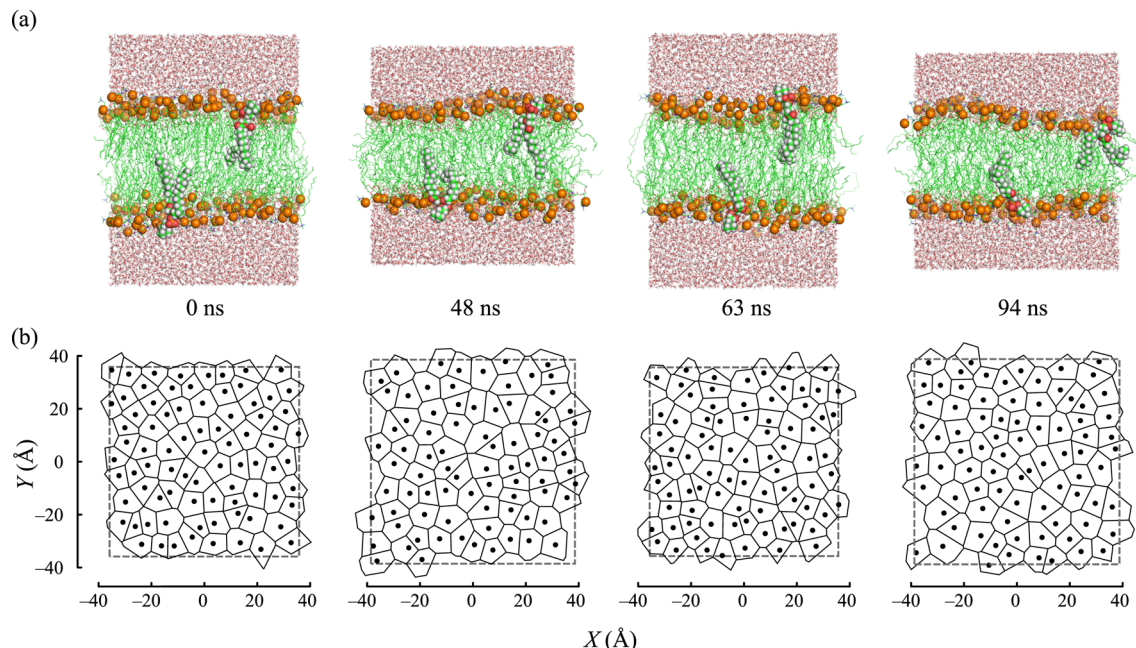


**Figure 1.** Representative snapshots in replica 1 of the  $\gamma$ -REMD simulation for the 162 DPPC lipid bilayer. (a) Structures of DPPC lipid bilayer. Orange spheres represent the phosphorus atoms in the lipid head groups. (b) Two-dimensional Voronoi tessellation for the centers-of-mass of the DPPC molecules in the upper leaflet of the bilayer.

In the  $\gamma$ -REMD simulation, we used six replicas, where target surface tensions were set to 0, 3.6, 7.2, 10.8, 14.4, and 18.0 dyn/cm, and all replicas have the same target temperature of 323.15 K and normal pressure of 1 atm. We performed 100 ns simulations for each replica, 600 ns in total, and replica exchange was tried every 100 ps. We used CHARMM c36 force-field parameters for DPPC lipids.<sup>51</sup> We employed the Langevin thermostat and barostat algorithms for temperature and pressure controls with the semi-isotropic pressure coupling.<sup>46,47</sup> The equations of motion were integrated by the leapfrog Verlet algorithm<sup>52,53</sup> with a time step of 2 fs, where we used SHAKE<sup>54</sup> and SETTLE<sup>55</sup> algorithms for bond constraints. For computation of nonbonded interactions, we used the particle mesh Ewald (PME) method<sup>56</sup> with the grid point of  $72 \times 72 \times 100$  and the linear  $1/R^2$  lookup table method,<sup>57</sup> where the Lennard-Jones potential was switched and truncated from 8 to 10 Å. We also performed the conventional MD simulations in the  $NP\gamma T$  ensemble ( $P = 1$  atm,  $T = 323.15$  K, and  $\gamma = 0, 3.6, 7.2, 10.8, 14.4$ , and 18.0 dyn/cm) for comparison. Note that simulations in the  $NP\gamma T$  ensemble at  $\gamma = 0$  dyn/cm also correspond to  $NPT$  simulations. All simulations were carried out with our in-house software, called GENESIS (GENeralized Ensemble SImulation System).<sup>58</sup>

**E. Simulation of the WALP23–POPC System.** WALP23 is a small transmembrane peptide with the amino acid sequence GWW(LA)<sub>8</sub>LWVA that has been widely used as a model protein for investigating the nature of hydrophobic mismatch between protein and lipids.<sup>59</sup> To explore the efficiency of conformational sampling of proteins in membranes, we performed  $\gamma$ -REMD simulations of a WALP23–POPC lipid bilayer and compared the results with those of MD simulations in the  $NPT$  ensemble. We modeled the initial structure by inserting a WALP23 peptide in the ideal  $\alpha$ -helical conformation ( $\phi = -57.8^\circ$ ;  $\psi = -47.0^\circ$ ), which was oriented perpendicular to the membrane, into a fully equilibrated 80 POPC lipid bilayer, followed by removal of overlapping lipid molecules. The system contained one WALP23 peptide, 38 lipids in the upper leaflet,

38 lipids in the lower leaflet, and 3666 TIP3P waters (total 21 558 atoms). The initial box size was  $(h_x, h_y, h_z) = (52.19 \text{ \AA}, 52.19 \text{ \AA}, 78.65 \text{ \AA})$ .

We gradually equilibrated the system in multiple steps, first a 10 000 step energy minimization, followed by 12 ns equilibration. For the first 250 ps, MD simulation in the  $NVT$  ensemble ( $T = 303.15$  K) was carried out with positional restraints on the heavy atoms of peptide and lipids. We then performed a 250 ps MD simulation in the  $NPAT$  ensemble ( $P = 1$  atm,  $T = 303.15$  K) with the same restraint potentials, followed by a 500 ps MD simulation with positional restraints on the peptide heavy atoms and the phosphorus atoms of the lipids. 11 ns MD simulations were then carried out in the  $NP\gamma T$  ensemble ( $P = 1$  atm and  $T = 303.15$  K) with positional restraints on the peptide heavy atoms (force constant = 1 kcal·mol<sup>-1</sup>·Å<sup>-2</sup>) to prepare the initial structure of each replica in the  $\gamma$ -REMD simulation.

In the  $\gamma$ -REMD simulation, we used five replicas, where the target surface tension was set to  $-10, -5, 0, +5$ , and  $+10$  dyn/cm for each replica, all having the same target temperature (303.15 K) and normal pressure (1 atm). We performed 100 ns simulations for each replica, during which replica exchange was tried every 100 ps. For the PME method, we used a grid point of  $54 \times 54 \times 80$ . The other parameters and algorithms used in this simulation were the same as in the 162 DPPC system. For WALP23, we used CHARMM c27 force-field parameters with  $\phi, \psi$  cross-term map correction (CMAP).<sup>60,61</sup> Trajectories of the first 20 ns were discarded for analysis of averaged quantities. All simulations were carried out with GENESIS.<sup>58</sup>

### III. RESULTS

**A. 162 DPPC System.** We performed  $\gamma$ -REMD simulation of the 162 DPPC lipid bilayer to ascertain the efficiency of this method for a simple biological membrane system. Figure 1a shows representative snapshots of the system obtained in replica 1 of the  $\gamma$ -REMD simulation. The lipid bilayer shrinks and stretches significantly along the membrane plane, changing in

thickness while keeping a planar shape. When thinner, the lipid tail groups are tilted and disordered, and when thicker are in extended conformations. In Figure 1b, we show the positions of the center-of-mass of the lipid molecules in each snapshot projected onto the  $xy$  plane, and the region occupied by each lipid is illustrated by a polygon, which was computed using the Voronoi tessellation algorithm.<sup>62,63</sup> Lipid molecules are distributed almost uniformly in spite of significant changes of the simulation box. In fact, there was neither collapse of the membrane nor formation of water pores in the membrane. Evidently, surface-tension exchange produces stable lateral deformation of lipid bilayers during simulation.

In the  $\gamma$ -REMD simulation, we expect a random walk of the target surface tension, which should lead to a random walk in area space of the lipid bilayers. To examine this, we analyzed the averaged area per lipid in the  $\gamma$ -REMD simulation and compared it with those in the MD simulations. The averaged area per lipid was calculated by dividing the area of the simulation box by the number of lipid molecules in one leaflet. Figure 2a shows the time courses of the averaged area per lipid in the MD simulations. The area fluctuated around  $64.3$  and  $70.3 \text{ \AA}^2$  at  $\gamma = 0$  and  $18 \text{ dyn/cm}$ , respectively. Figure 2b shows the time series of the replica number at  $\gamma = 0 \text{ dyn/cm}$  in the  $\gamma$ -REMD simulation. We can see that the surface tension randomly visits each replica, demonstrating that a random walk in the surface tension space is successfully realized. Parts c and d of Figure 2 show the time courses of the target surface tension and averaged area per lipid in replica 1 of the  $\gamma$ -REMD simulation. The averaged area per lipid changes significantly, fluctuating between and around the averaged values at  $\gamma = 0$  and  $18 \text{ dyn/cm}$  of the MD simulations (shown by dashed lines in the figure). As expected, the area increases as the target surface tension increases, and vice versa. We suggest that the  $\gamma$ -REMD method enforces a random walk in area space.

We also analyzed the membrane thickness, which is computed from the distance between the averaged positions of the phosphorus atoms of lipid head groups in each leaflet. In the MD simulations, the membrane thickness fluctuated around  $38.0$  and  $35.5 \text{ \AA}$  at  $\gamma = 0$  and  $18 \text{ dyn/cm}$ , respectively (Figure 3a), whereas in the  $\gamma$ -REMD simulation it changed significantly between and around these values (Figure 3b). The opposite tendency to the area per lipid was observed (compare Figures 2d and 3b); namely, thickness decreases as the target surface tension increases, and vice versa, which is due to volume incompressibility of the membrane. Evidently, a random walk in thickness space is also realized in  $\gamma$ -REMD simulations.

We analyzed the probability distributions of potential energy, volume, and area (or area per lipid). It was found that the distributions of potential energy and volume in the  $\gamma$ -REMD simulation coincide with those in the MD simulations (Figure S1 in the Supporting Information). As for the area, distributions at  $\gamma = 0 \text{ dyn/cm}$  in the  $\gamma$ -REMD and MD simulations were in agreement with each other, whereas the distribution at  $\gamma = 18 \text{ dyn/cm}$  in the  $\gamma$ -REMD simulation was slightly shifted upward to higher areas by  $\sim 1 \text{ \AA}^2$  per lipid. The  $\gamma$ -REMD algorithms may untangle intertwined acyl chains of lipids, making the membrane more flexible. Because all the data showed a bell-shaped distribution, phase transitions of the lipid bilayer do not occur in these conditions. There was enough overlap between all neighboring pairs of the distributions of the area. The acceptance ratio in the Metropolis criteria was  $0.529$ ,  $0.484$ ,  $0.555$ ,  $0.502$ , and  $0.481$  for  $\gamma_1 \leftrightarrow \gamma_2$ ,  $\gamma_2 \leftrightarrow \gamma_3$ ,  $\gamma_3 \leftrightarrow \gamma_4$ ,  $\gamma_4 \leftrightarrow \gamma_5$ , and  $\gamma_5 \leftrightarrow \gamma_6$ , respectively, demonstrating that there is good surface-tension exchange between pairs of replicas.

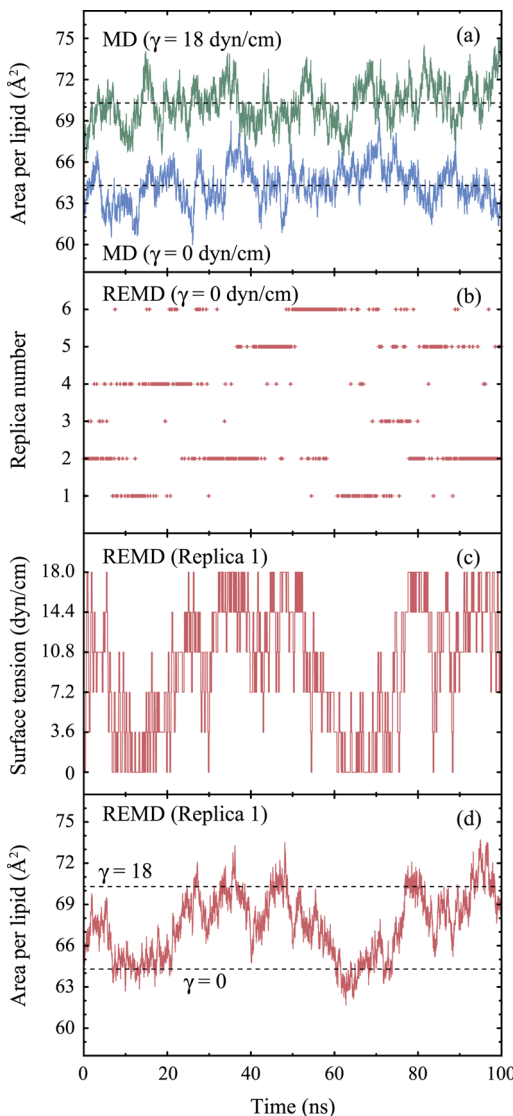


**Figure 2.** Time courses of the averaged area per lipid of DPPC lipid bilayers, replica number, and target surface tension in MD and  $\gamma$ -REMD simulations. (a) Averaged area per lipid in the MD simulation at  $\gamma = 0 \text{ dyn/cm}$  (blue line) and  $\gamma = 18 \text{ dyn/cm}$  (green line). (b) Replica number at  $\gamma = 0 \text{ dyn/cm}$  in the  $\gamma$ -REMD simulation. (c) Target surface tension in replica 1 of the  $\gamma$ -REMD simulation. (d) Averaged area per lipid in replica 1 of the  $\gamma$ -REMD simulation. Dashed lines in (a) and (d) represent the time-averaged area per lipid obtained from the MD simulations at  $\gamma = 0$  and  $18 \text{ dyn/cm}$ .

We calculated the averaged value of the structural parameters of the lipid bilayer in the MD and  $\gamma$ -REMD simulations. We analyzed the area per lipid, membrane thickness, order parameter, and electron density profile, using the WHAM technique (eqs 13–15) to obtain averaged values in the REMD simulation. The order parameter was calculated by

$$S_{CD} = \frac{1}{2}(3 \cos^2 \theta - 1) \quad (19)$$

where  $\theta$  is the angle between the C–H bond in the lipid acyl chains and the bilayer normal. The electron density profiles were computed from the trajectories by dividing the simulation box into  $0.1 \text{ \AA}$  slabs and determining the averaged number of electrons in each slab. As expected, higher surface tension increased the area per lipid while decreasing the membrane thickness and

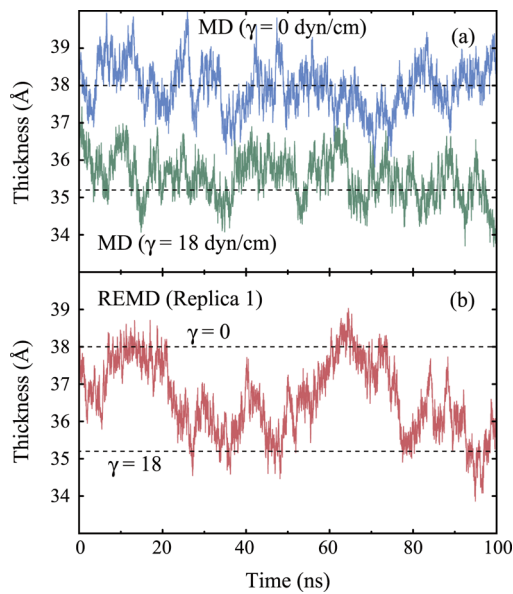


**Figure 3.** Time courses of the membrane thickness of the DPPC lipid bilayer in MD and  $\gamma$ -REMD simulations. (a) Membrane thickness in the MD simulation at  $\gamma = 0$  dyn/cm (blue solid line) and  $\gamma = 18$  dyn/cm (green line). (b) Membrane thickness in Replica 1 of the  $\gamma$ -REMD simulation. Dashed lines in (a) and (b) represent the time-averaged membrane thickness obtained from the MD simulations at  $\gamma = 0$  and 18 dyn/cm.

acyl chain order. In the  $\gamma$ -REMD simulation, the averaged area per lipid at  $\gamma = 0$ , 3.6, 7.2, 10.8, 14.4, and 18.0 dyn/cm was 64.1, 65.2, 66.5, 67.8, 69.2, and 70.9 Å<sup>2</sup>, respectively. The corresponding averaged membrane thickness was 38.0, 37.5, 37.0,

36.5, 35.9, and 35.2 Å, respectively. Similar results were obtained in the MD simulations (Table S1 in the Supporting Information). The order parameters of acyl chains and electron density profiles of the water phase as well as lipid components were also consistent between MD and  $\gamma$ -REMD simulations (Figure 4a,b). These results indicate that the averaged structures of the lipid bilayer obtained by the  $\gamma$ -REMD simulation are in good agreement with those of MD simulations. Importantly, the convergence of these structural parameters in the  $\gamma$ -REMD simulation was faster than in the MD simulations (40 ns compared with 75 ns) (Figure 4c). Electron density profiles also showed a similar convergence (Figure 4d). We conclude that sampling of equilibrium structures of the lipid bilayer is more efficient in  $\gamma$ -REMD simulations.

We further analyzed dynamic properties of DPPC lipids in the  $\gamma$ -REMD simulation. Intuitively, one expects that large fluctuations in the area of the system would enhance lateral movement of lipids. To examine this, we calculated the two-dimensional mean-square displacement (MSD) of the center-of-mass (COM) position of lipid molecules at  $\gamma = 0$  dyn/cm. The MSD is calculated by

$$\text{MSD}(t) = \langle |\mathbf{r}(t' + t) - \mathbf{r}(t')|^2 \rangle \quad (20)$$

where  $\mathbf{r}(t)$  is the  $x, y$  position of the COM of a lipid at time  $t$ , and the brackets denote averaging over all lipids and time origins  $t'$ . As suggested by Klauda et al.,<sup>64</sup> motion of the COM of the entire system was removed to compute the position of each lipid molecule (Klauda's method). We calculated the MSD for each replica based on eq 20, using only the coordinates at  $\gamma = 0$  dyn/cm. The lateral diffusion constant obtained from the MD simulation at  $\gamma = 0$  dyn/cm ( $0.68 \times 10^{-7}$  cm<sup>2</sup>/s for >10 ns) is close to experimental data<sup>65</sup> as well as

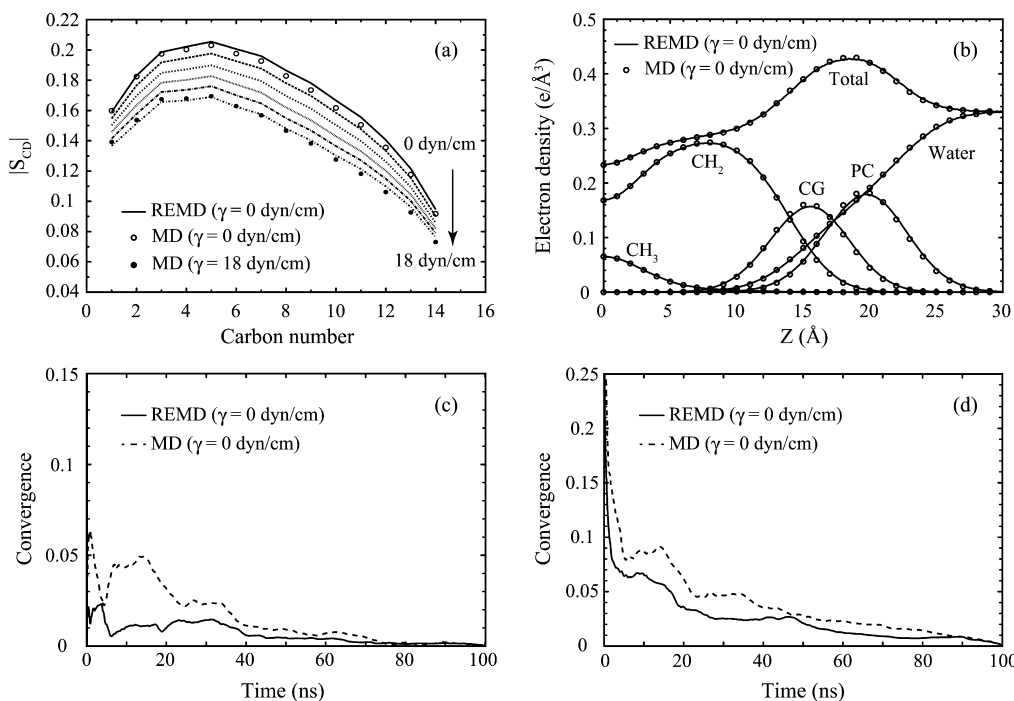


**Figure 4.** Analysis of structural parameters of the 162 DPPC lipid bilayer in  $\gamma$ -REMD and MD simulations. (a) Order parameter of C–H bonds in the acyl chains. Lines are from the  $\gamma$ -REMD simulations at  $\gamma = 0$ , 3.6, 7.2, 10.6, 14.4, and 18 dyn/cm (from top to bottom). (b) Electron density profiles of lipid components (PC, phosphate-choline; CG, carbonyl-glycerol; CH<sub>2</sub>, ethyl group, and CH<sub>3</sub>, methyl group, in acyl chains) and water molecules. (c) Convergence of order parameter at  $\gamma = 0$  dyn/cm. (d) Convergence of electron density for lipid + water phases (total) at  $\gamma = 0$  dyn/cm. Convergence at each step was defined as the root-mean-square deviation between the data averaged from 0 ns to each step and the data averaged over 100 ns.

other simulation data.<sup>64</sup> Interestingly, in the  $\gamma$ -REMD simulation all replicas showed larger MSD compared to the MD simulation (Figure 5), indicating accelerated lipid lateral

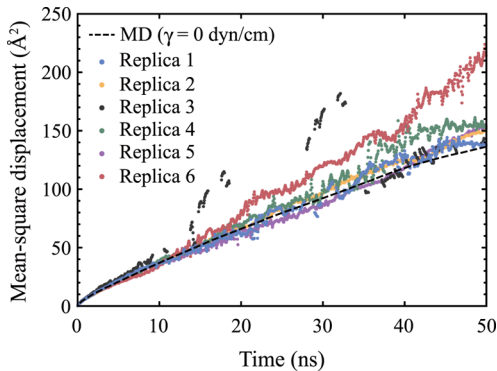


**Figure 5.** Mean-square-displacement of the  $x, y$  position of the center-of-mass of DPPC lipids at  $\gamma = 0$  dyn/cm in the  $\gamma$ -REMD (points) and MD simulations (dashed line).

diffusion. Here, the MSD for replica 3 showed relatively large deviations from others, presumably due to the small number of sampled coordinates in this replica (Figure 2b). We further examined the MSD on the basis of another method proposed by Anezo et al.,<sup>66</sup> in which the COM drift of each leaflet is removed to compute the position of each lipid molecule (Anezo's method). Accelerated lipid lateral diffusion was still observed (Figure S2 in the Supporting Information).

An increase in lateral diffusion is readily explained by free-area theory.<sup>67</sup> According to this theory, lipid molecules can hop from one cage to another given enough neighboring void space. Because surface tension increases the exposed surface area of the bilayer, it follows that the appropriately sized void space must open more frequently. In fact, lateral diffusion obtained in the MD simulations at  $\gamma = 3.6, 7.2, 10.6, 14.4$ , and 18 dyn/cm was larger than those at  $\gamma = 0$  dyn/cm (Figure S3 in the Supporting Information), which is also consistent with other recent MD simulations of lipid bilayers under surface tension.<sup>68,69</sup> We suggest that randomly applied surface tension enhances lateral diffusion of lipid molecules, thereby providing greater sampling of “mixed” configurations of lipids in the  $\gamma$ -REMD simulation compared to conventional MD simulations—an important consequence of the  $\gamma$ -REMD method.

Finally, we analyzed lipid reorientation, especially rotational motion of lipid body and headgroup. The relaxation rate of reorientation is given by the correlation function:

$$C_2(t) = \langle P_2(\hat{\mu}(t') + t) \cdot \hat{\mu}(t') \rangle \quad (21)$$

where  $P_2$  is the second Legendre polynomial  $1/2(3x^2 - 1)$  and  $\hat{\mu}$  is a certain unit vector between two atoms in the lipid molecule.<sup>70</sup> Here, we used the vector between phosphorus and nearby hydrogens (HA atom in the glycerol backbone and H11A atom in the chorine group) to capture the rotational motion of the lipid body and headgroup. For the  $\gamma$ -REMD trajectories, the average in eq 21 was taken over coordinates at  $\gamma = 0$  dyn/cm. We observed that the correlation function converged within 5–10 ns in both  $\gamma$ -REMD and MD simulations (Figure S4 in the Supporting Information). Interestingly,  $\gamma$ -REMD showed approximately the same relaxation rate as MD at 0 dyn/cm, whereas MD at 18 dyn/cm showed quicker relaxation than at 0 dyn/cm. This is presumably due to the fact that the time scale of lipid reorientation is much faster than that of area change induced by surface-tension exchange, making the effects of the  $\gamma$ -REMD algorithm invisible. During the MD simulation at  $\gamma = 18$  dyn/cm, the area in the system is always expanded, allowing a faster relaxation rate compared with MD at  $\gamma = 0$  dyn/cm. We suggest that enhanced sampling by the  $\gamma$ -REMD method is realized for dynamic properties with time scales longer than 5 ns.

**B. WALP23–POPC System.** To explore sampling efficiency of the  $\gamma$ -REMD algorithm for protein-membrane systems, we performed simulations of a WALP23 peptide in an explicit POPC lipid bilayer. As in the 162 DPPC simulation, we observed that the POPC lipid bilayer shrinks and stretches significantly along the membrane plane. Figure 6 shows representative snapshots obtained in Replica 4 of the  $\gamma$ -REMD simulation. In spite of large deformation of the membrane, the structure of WALP23 is stable during the simulation, keeping the  $\alpha$ -helical conformation without significant bending or kinks. The root-mean-square deviation (RMSD) from the initial structure with respect to the  $C^\alpha$  atoms was less than 3.0 Å for 100 ns in each replica. WALP23 reorients repeatedly during the simulation. This dynamic behavior of the peptide presumably derives from hydrophobic mismatch between the peptide and lipids coupled with large lateral deformation of the membrane induced by the  $\gamma$ -REMD algorithm.

During the  $\gamma$ -REMD simulation, we observed a random walk in area space as well as surface tension space. The area increased

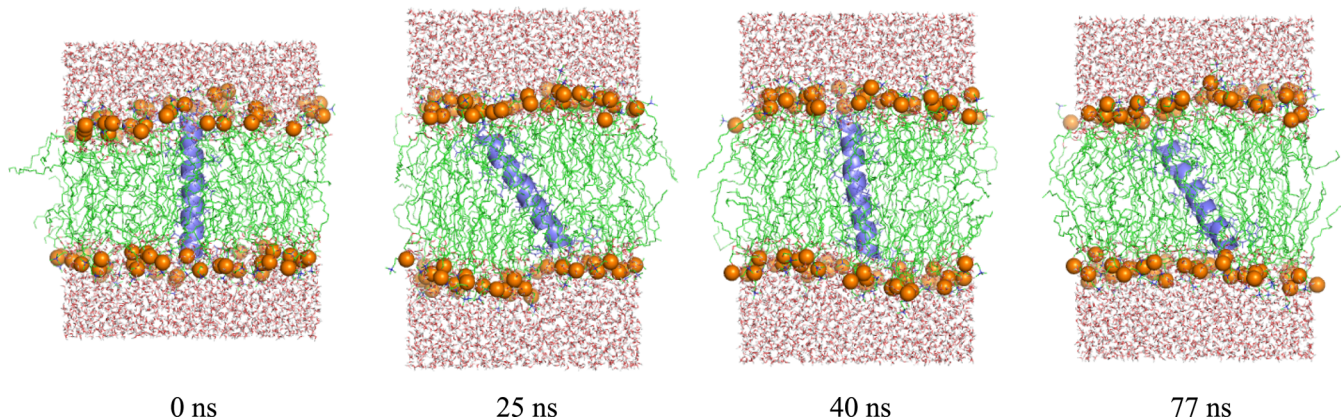


**Figure 6.** Representative snapshots in replica 4 of the  $\gamma$ -REMD simulation for the WALP23–POPC lipid bilayer. All snapshots are viewed from the same side.

as the target surface tension increased, and vice versa (Figure S5 in the Supporting Information). The potential energy, volume, and area of the system showed bell-shaped distributions at each surface tension condition, and there was enough overlap of area distributions between all neighboring pairs (Figure S6 in the Supporting Information). The acceptance ratio in the Metropolis criteria was 0.623, 0.556, 0.585, and 0.562 for  $\gamma_1 \leftrightarrow \gamma_2$ ,  $\gamma_2 \leftrightarrow \gamma_3$ ,  $\gamma_3 \leftrightarrow \gamma_4$ , and  $\gamma_4 \leftrightarrow \gamma_5$ , respectively, demonstrating that there was efficient surface-tension exchange between pairs of replicas.

We investigated relationships between membrane thickness, peptide tilt angle, and target surface tension. Membrane thickness changed more significantly in the  $\gamma$ -REMD simulation compared with in the MD simulation (Figure S7a,b in the Supporting Information). These large changes in the membrane thickness were coupled with changes in surface area due to volume incompressibility of the membrane. We analyzed the peptide tilt angle, which was computed from the helix axis that maximizes the summation of inner products between a vector in the helix itself and CO/NH vectors in the backbone. Again, we observed significant changes of the tilt angle in the  $\gamma$ -REMD simulation (Figure S7c,d in the Supporting Information). Importantly, it was found that the tilt angle tends to increase as the membrane thickness decreases (Figure S7e,f in the Supporting Information), indicating the effects of hydrophobic mismatch between peptide and membrane. In the  $\gamma$ -REMD simulation, the averaged tilt angle at  $\gamma = -10, -5, 0, +5$ , and  $+10$  dyn/cm was  $15.9, 16.7, 17.9, 19.4$ , and  $21.0^\circ$ , respectively, and the averaged membrane thickness was  $39.6, 39.2, 38.7, 38.2$ , and  $37.6$  Å, respectively. These results indicate that  $\gamma$ -REMD algorithms enhanced changes in the membrane thickness and facilitated reorientation of WALP23 through protein–lipid interactions.

We compared the sampling efficiency of the peptide tilt angle between  $\gamma$ -REMD and MD simulations. Histograms of the tilt angle obtained at  $\gamma = 0$  dyn/cm in the two simulations are shown in Figure 7a, where the data of the first 20 ns were excluded from the analysis. We can see that the  $\gamma$ -REMD simulation sampled a much wider range of tilt angle than the MD simulation ( $0$ – $40^\circ$  compared with  $5$ – $30^\circ$ , respectively). Finally, we computed the potential of mean force (PMF) as a function of tilt angle (using eqs 16–18 for  $\gamma$ -REMD, and eq 16 for MD), and the results are shown in Figure 7b. The free energy landscape obtained from the  $\gamma$ -REMD simulation has a parabolic shape, with the global energy minimum located at  $18^\circ$ . The energy surface is almost flat around  $18^\circ$ , and the energy increases as the tilt angle decreases ( $<10^\circ$ ) or increases ( $>30^\circ$ ). These characteristics are consistent with results obtained from umbrella sampling simulations for the WALP peptides in POPC lipid bilayers reported by Kim and Im.<sup>71</sup>

There is an entropic cost in the small tilt angle region and unfavorable interaction between peptide and lipids in the large angle region.<sup>71</sup> As a result, in the conventional MD simulation, the range of thermally accessible tilt angles of WALP23 is narrow ( $5$ – $30^\circ$ ). On the other hand, in our  $\gamma$ -REMD method such energetic costs in the small and large tilt angle regions are lowered due to hydrophobic mismatch at negative or positive target surface tension conditions, allowing for a much wider range of orientations of the peptide to be sampled. We believe our method is useful for computation of free energy profile of more complex protein-membrane systems.

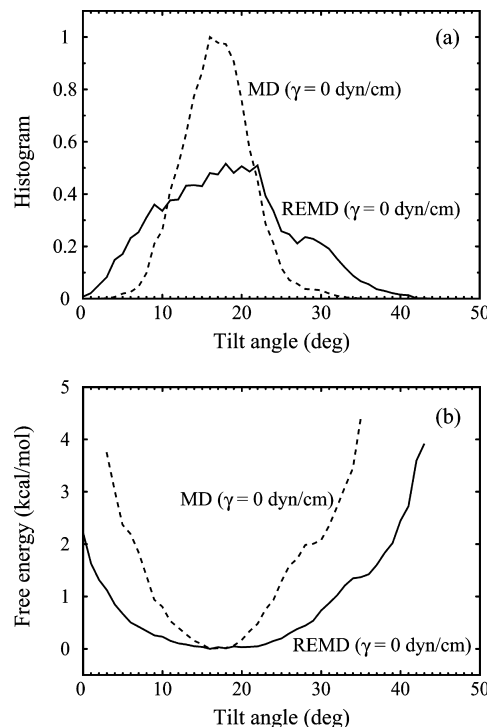


**Figure 7.** Histogram and potential of mean force as a function of tilt angle of WALP23. (a) Histogram of the tilt angle in MD (dashed line) compared with that in  $\gamma$ -REMD (solid line). (b) Potential of mean force as a function of tilt angle obtained from MD (dashed line) and  $\gamma$ -REMD (solid line) simulations.

#### IV. DISCUSSION

The setup procedure for the  $\gamma$ -REMD simulation is simple. First, the minimum and maximum values of the target surface tension to be used are decided. According to the previous MD simulations in the  $NP\gamma T$  ensemble,  $10$ – $20$  dyn/cm was found to be reasonable as the maximum target surface tension for stable  $\gamma$ -REMD simulation of phospholipid bilayers. The minimum value is normally set to  $0$  dyn/cm, which corresponds to the  $NPT$  ensemble. In the  $\gamma$ -REMD simulation of the WALP23–POPC system, we also used negative surface tensions to simulate thicker membranes. Intermediate surface tensions are chosen so that enough overlap in area distributions is obtained, because the extent of overlap dictates the efficiency of surface-tension exchange. Because the increase in lipid surface area is almost proportional to the increase in surface tension, we assigned target surface tensions to intermediate replicas linearly between the maximum and minimum values. In this study, we used six and five replicas for 162 DPPC and WALP23–POPC systems, respectively. Larger systems require more replicas, but we do not anticipate a drastic increase in the number.

Recently, Klauda et al. reported a finite size effect on lipid diffusion and this is especially evident in smaller membrane systems.<sup>64</sup> A  $\gamma$ -REMD simulation of a 72 DPPC system indeed exhibited such anomalies, in that we obtained about a 3 times larger diffusion constant compared with the 162 DPPC system. In addition, we found that the diffusion constant decreased as the target surface tension increased when the system was analyzed by Klauda's method, whereas the opposite was the case with the Anezo's method (Figures S8 in the Supporting Information). This contradiction might be due to the fact that in a small system

finite size effects, which can be weakened at a higher surface tension condition, because it increases the system area, are still stronger than the effects (acceleration of diffusion) induced by the  $\gamma$ -REMD algorithm, whereas accelerated diffusion can emerge if finite size effects are partially removed by the Anezo's method. In the  $\gamma$ -REMD simulation of 72 DPPC, however, analysis of statistical, structural, and dynamic properties of the lipid bilayers except for the lateral diffusion showed the same results with those of 162 DPPC (Table S2 and Figures S9–S15 in the Supporting Information). We suggest that the  $\gamma$ -REMD method is useful even for smaller membrane systems, whereas in such a simulation we should not focus on the lipid diffusion but on other properties in the system.

Our surface-tension REMD method will be applicable to a wide variety of biological membrane systems. We anticipate use in more complex applications, such as protein-membrane and mixed bilayer systems. Protein–lipid interactions, consisting of electrostatic, hydrogen-bonding, and hydrophobic interactions, are crucial to the stability and activity of membrane proteins and are readily sampled by our method. Annular lipids, i.e., those immediately surrounding the protein, which have different structural and dynamic properties compared to bulk lipids, have great influence and need special attention.<sup>4</sup> Because diffusion of annular lipids is suppressed due to perturbations by membrane proteins, enhancing lipid diffusion by surface-tension exchange is a useful way to sample the conformations of annular lipids. Recently, several different methods and models have been proposed for enhanced sampling. As an example, Wang et al., developed an accelerated MD method with a boost potential inducing *trans-gauche* isomerization of lipid acyl chains, resulting in the accelerated lipid lateral diffusion.<sup>72</sup> A combination of surface-tension REMD and accelerated MD methods will likely expand conformational sampling.

Large-scale conformational changes of membrane proteins can be explored more thoroughly by the surface-tension REMD method. Many membrane proteins change their shape or conformation during function, and protein–lipid interactions often play an important role. For example, the mechanosensitive ion channel (MscL) opens and closes its pore in response to membrane tension.<sup>73</sup> The protein-conducting channel (SecY) undergoes conformational transitions between closed, pre-open, and open states, where lateral movement of proximal lipids is essential to stabilize the preopen form.<sup>74,75</sup> We speculate that such large conformational changes of membrane proteins may be facilitated by deformation of the membrane and/or by enhanced lateral diffusion of proximal lipids via protein–lipid interactions.

Our method may allow efficient exploration of mixed lipid bilayer systems like lipid rafts, which are membrane subdomains rich in cholesterol and sphingolipids.<sup>6,7</sup> They are involved in a number of cellular processes like signal transduction, membrane trafficking, and immune responses. Little is known about their structures. Because such a complex system has many possible configurations, enhanced sampling may be essential for reliable simulations and therefore understanding of their structures. Our surface-tension REMD method will be useful to analyze interactions between component molecules in mixed lipid bilayer systems.

## V. SUMMARY

In this study, we developed a new generalized-ensemble algorithm, called the surface-tension REMD method. We applied

the method to a fully hydrated DPPC lipid bilayer system and a WALP23–POPC lipid bilayer system. We observed significant lateral deformations of the membrane without collapse of the lipid bilayer structure during simulation. We also found that in the surface-tension REMD simulation random walks in not only area space but also thickness space are realized, and structural sampling is enhanced compared to conventional MD simulations. Our method promises to be useful in the simulation of various cellular processes taking place at membrane interfaces. Our future studies will focus on simulation of more complex protein-membrane systems.

## APPENDIX

In this Appendix, we present derivations of eq 11 in the case where we use the Langevin dynamics method as the constant temperature–pressure algorithm.<sup>46,47</sup> In the Langevin dynamics method for a fully flexible simulation cell, the equation of motion for a system of  $N$  atoms is given by

$$\begin{aligned} \frac{d\mathbf{r}_i}{dt} &= \frac{\mathbf{p}_i}{m_i} + \frac{\tilde{\mathbf{p}}_e}{W}\mathbf{r}_i \\ \frac{d\mathbf{p}_i}{dt} &= \mathbf{F}_i - \frac{\tilde{\mathbf{p}}_e}{W}\mathbf{p}_i - \frac{1}{3N}\frac{\text{Tr}[\tilde{\mathbf{p}}_e^2]}{W}\mathbf{p}_i - \gamma_t\mathbf{p}_i + \mathbf{R}_i \\ \frac{d\tilde{\mathbf{h}}}{dt} &= \frac{\tilde{\mathbf{p}}_e}{W}\tilde{\mathbf{h}} \\ \frac{d\tilde{\mathbf{p}}_e}{dt} &= V(\tilde{\mathbf{P}}_{\text{int}} - \tilde{\mathbf{I}}P_{\text{ext}}) + \left[ \frac{1}{3N} \sum_{i=1}^N \frac{\mathbf{p}_i^2}{m_i} \right] \tilde{\mathbf{I}} - \gamma_p \tilde{\mathbf{p}}_e + \tilde{\mathbf{R}}_p \end{aligned} \quad (\text{A1})$$

where  $\mathbf{r}_i$  and  $\mathbf{p}_i$  are the position and momentum of the  $i$ th atom,  $\tilde{\mathbf{h}}$  is the matrix of cell parameters,  $\tilde{\mathbf{p}}_e$  is the matrix of barostat momenta,  $\mathbf{F}_i$  is the force,  $m_i$  is the mass of the  $i$ th atom,  $V$  is the volume,  $P_{\text{ext}}$  is the external pressure,  $\tilde{\mathbf{P}}_{\text{int}}$  is the internal pressure tensor, and  $\tilde{\mathbf{I}}$  is the identity matrix.  $\gamma_t$  is a friction coefficient representing viscous damping due to fictitious heat bath particle, and  $\gamma_p$  is a friction coefficient for the barostat.  $W$  is the barostat mass given by

$$W = \frac{3Nk_B T}{(2\pi\gamma_p)^2} \quad (\text{A2})$$

where  $T$  is the temperature.  $\mathbf{R}_i$  is the random force acting on the  $i$ th atom that satisfies the fluctuation–dissipation theorem:  $\langle R_i(t) R_j(t') \rangle = 2m_i\gamma_t k_B T \delta(t-t')$ , where  $\delta(t-t')$  is the Dirac delta function and brackets mean the average over time.  $R_i(t)$  has a Gaussian distribution with zero mean and variance of  $(2m_i\gamma_t k_B T / \Delta t)^{1/2}$ .  $R_p$  is the random force acting on the barostat, which also follows a Gaussian distribution with zero mean and variance of  $(2W\gamma_p k_B T / \Delta t)^{1/2}$ .

In the *NPT* ensemble for the orthorhombic cell, the probability of finding the system in the state  $x = (q, p, p_e, h)$  is given by the distribution function:<sup>47</sup>

$$\begin{aligned} f(x) = C \exp &\left[ -\beta \left\{ K(p) + E(q, h) + P_{\text{ext}} h_x h_y h_z \right. \right. \\ &\left. \left. + \frac{1}{2W} \text{Tr}[\tilde{\mathbf{p}}_e^T \tilde{\mathbf{p}}_e] \right\} \right] \end{aligned} \quad (\text{A3})$$

where  $C$  is a normalization constant,  $K$  is the kinetic energy, and  $E$  is the potential energy.

In the  $N\bar{P}\gamma T$  ensemble, we use the following equation for  $\frac{dp_e}{dt}$  instead of that in eq A1:

$$\left( \frac{dp_e}{dt} \right)_{\alpha\beta} = \begin{cases} V[(\vec{\mathbf{p}}_{\text{int}})_{\alpha\alpha} - P_{\text{ext}}] + \gamma_{\text{ext}} A_{xy} + \frac{1}{3N} \sum_{i=1}^N \frac{\mathbf{p}_i^2}{m_i} - \gamma_p (\vec{\mathbf{p}}_e)_{\alpha\alpha} + (\vec{\mathbf{R}}_p)_{\alpha\alpha} & (\alpha = \beta) = x \text{ or } y \\ V[(\vec{\mathbf{p}}_{\text{int}})_{zz} - P_{\text{ext}}] + \frac{1}{3N} \sum_{i=1}^N \frac{\mathbf{p}_i^2}{m_i} - \gamma_p (\vec{\mathbf{p}}_e)_{zz} + (\vec{\mathbf{R}}_p)_{zz} & (\alpha = \beta) = z \\ 0 & \alpha \neq \beta \end{cases} \quad (\text{A4})$$

where  $A_{xy}$  is the area of the simulation cell and  $\gamma_{\text{ext}}$  is the external surface tension.<sup>76</sup> If  $\gamma_{\text{ext}} = 0$ , eq A4 is equivalent to eq A1 in the  $NPT$  ensemble for the orthorhombic cell.

In the  $N\bar{P}\gamma T$  ensemble, the distribution function is given by

$$f(x) = C \exp \left[ -\beta \left\{ K(p) + E(q, h) + P_{\text{ext}} h_x h_y h_z - \gamma_{\text{ext}} h_x h_y \right. \right. \\ \left. \left. + \frac{1}{2W} \text{Tr}[\vec{\mathbf{p}}_e^t \vec{\mathbf{p}}_e] \right\} \right] \quad (\text{A5})$$

We now consider exchanging a pair of replicas in the generalized ensemble, where each replica is simulated in the  $N\bar{P}\gamma T$  ensemble with the Langevin dynamics method. Suppose a

pair of replicas  $i$  and  $j$  are exchanged, and let  $X'$  be a state after the replicas are exchanged as in eq 5:

$$X = \{ \dots, x_m^{[i]}, \dots, x_n^{[j]}, \dots \} \rightarrow X' = \{ \dots, x_m^{[j]}, \dots, x_n^{[i]}, \dots \} \quad (\text{A6})$$

We define  $x_n^{[i]'}$  and  $x_m^{[j]'} by the following forms:$

$$\begin{cases} x_n^{[i]'} = (q^{[i]}, p^{[i]}, p_e^{[i]}, h^{[i]})_n \\ x_m^{[j]'} = (q^{[j]}, p^{[j]}, p_e^{[j]}, h^{[j]})_m \end{cases} \quad (\text{A7})$$

Using eqs 8, 9, A5, and A7, the detailed balance condition is written as

$$w(X \rightarrow X') C_m \exp \left[ -\beta_m \left\{ K(p^{[i]}) + E(q^{[i]}, h^{[i]}) + P_m h_x^{[i]} h_y^{[i]} h_z^{[i]} - \gamma_m h_x^{[i]} h_y^{[i]} + \frac{1}{2W_m} \text{Tr}[\vec{\mathbf{p}}_e^{t[i]} \vec{\mathbf{p}}_e^{[i]}] \right\} \right] \\ \times C_n \exp \left[ -\beta_n \left\{ K(p^{[j]}) + E(q^{[j]}, h^{[j]}) + P_n h_x^{[j]} h_y^{[j]} h_z^{[j]} - \gamma_n h_x^{[j]} h_y^{[j]} + \frac{1}{2W_n} \text{Tr}[\vec{\mathbf{p}}_e^{t[j]} \vec{\mathbf{p}}_e^{[j]}] \right\} \right] \\ = w(X' \rightarrow X) C_m \exp \left[ -\beta_m \left\{ K(p^{[j]}) + E(q^{[j]}, h^{[j]}) + P_m h_x^{[j]} h_y^{[j]} h_z^{[j]} - \gamma_m h_x^{[j]} h_y^{[j]} + \frac{1}{2W_m} \text{Tr}[\vec{\mathbf{p}}_e^{t[j]} \vec{\mathbf{p}}_e^{[j]}] \right\} \right] \\ \times C_n \exp \left[ -\beta_n \left\{ K(p^{[i]}) + E(q^{[i]}, h^{[i]}) + P_n h_x^{[i]} h_y^{[i]} h_z^{[i]} - \gamma_n h_x^{[i]} h_y^{[i]} + \frac{1}{2W_n} \text{Tr}[\vec{\mathbf{p}}_e^{t[i]} \vec{\mathbf{p}}_e^{[i]}] \right\} \right] \quad (\text{A8})$$

If the momenta of atoms  $p^{[i]'}_e$  and  $p^{[j]'}_e$  are rescaled by

$$p^{[i]'}_e = \sqrt{\frac{T_n}{T_m}} p^{[i]}_e \quad p^{[j]'}_e = \sqrt{\frac{T_m}{T_n}} p^{[j]}_e \quad (\text{A9})$$

and barostat momenta  $p^{[i]'}_e$  and  $p^{[j]'}_e$  are rescaled by

$$p^{[i]'}_e = \sqrt{\frac{T_n W_n}{T_m W_m}} p^{[i]}_e \quad p^{[j]'}_e = \sqrt{\frac{T_m W_m}{T_n W_n}} p^{[j]}_e \quad (\text{A10})$$

the detailed balance condition of eq A8 is rewritten as

$$w(X \rightarrow X') \exp \left[ -\beta_m \left\{ K(p^{[i]}) + E(q^{[i]}, h^{[i]}) + P_m h_x^{[i]} h_y^{[i]} h_z^{[i]} - \gamma_m h_x^{[i]} h_y^{[i]} + \frac{1}{2W_m} \text{Tr}[\vec{\mathbf{p}}_e^{t[i]} \vec{\mathbf{p}}_e^{[i]}] \right\} \right] \\ \times \exp \left[ -\beta_n \left\{ K(p^{[j]}) + E(q^{[j]}, h^{[j]}) + P_n h_x^{[j]} h_y^{[j]} h_z^{[j]} - \gamma_n h_x^{[j]} h_y^{[j]} + \frac{1}{2W_n} \text{Tr}[\vec{\mathbf{p}}_e^{t[j]} \vec{\mathbf{p}}_e^{[j]}] \right\} \right] \\ = w(X' \rightarrow X) \exp \left[ -\beta_m \left\{ \frac{T_m}{T_n} K(p^{[j]}) + E(q^{[j]}, h^{[j]}) + P_m h_x^{[j]} h_y^{[j]} h_z^{[j]} - \gamma_m h_x^{[j]} h_y^{[j]} + \frac{T_m W_m}{T_n W_n} \frac{1}{2W_m} \text{Tr}[\vec{\mathbf{p}}_e^{t[j]} \vec{\mathbf{p}}_e^{[j]}] \right\} \right] \\ \times \exp \left[ -\beta_n \left\{ \frac{T_n}{T_m} K(p^{[i]}) + E(q^{[i]}, h^{[i]}) + P_n h_x^{[i]} h_y^{[i]} h_z^{[i]} - \gamma_n h_x^{[i]} h_y^{[i]} + \frac{T_n W_n}{T_m W_m} \frac{1}{2W_n} \text{Tr}[\vec{\mathbf{p}}_e^{t[i]} \vec{\mathbf{p}}_e^{[i]}] \right\} \right] \quad (\text{A11})$$

The kinetic energy terms in this equation are canceled out, and then we obtain eq 11.

## ■ ASSOCIATED CONTENT

### Supporting Information

Supporting Information includes the following: Computational details of the  $\gamma$ -REMD simulation of the 72 DPPC lipid bilayer; averaged area per lipid and membrane thickness in the  $\gamma$ -REMD and MD simulations of 162 DPPC (Table S1) and 72 DPPC lipid bilayer systems (Table S2); probability distributions of the potential energy, volume, and area of 162 DPPC (Figure S1); MSD of the  $x, y$  position of the COM of lipids in the  $\gamma$ -REMD simulation of 162 DPPC computed with Anezo's method (Figure S2); MSD of the  $x, y$  position of the COM of lipids in the MD simulation of 162 DPPC at  $\gamma = 0$ –18.0 dyn/cm (Figure S3); reorientation correlation functions of phosphorus and nearby hydrogen vectors obtained from 162 DPPC (Figure S4); time courses of the replica number, target surface tension, and system area in the  $\gamma$ -REMD simulation of WALP23–POPC (Figure S5); probability distributions of the potential energy, volume, and area of WALP23–POPC obtained from the  $\gamma$ -REMD simulation (Figure S6); analysis of POPC bilayer thickness and tilt angle of WALP23 (Figure S7); MSD of the  $x, y$  position of the COM of lipids in the  $\gamma$ -REMD and MD simulations of 72 DPPC (Figure S8). Other results of the  $\gamma$ -REMD and MD simulations of 72 DPPC lipid bilayers are shown in Figures S9–S15, which were obtained from the same analysis used for 162 DPPC and correspond to Figures 1–5 and Figures S1–4. This information is available free of charge via the Internet at <http://pubs.acs.org/>.

## ■ AUTHOR INFORMATION

### Corresponding Author

\*Y. Sugita: phone, +81-48-462-1407; fax, +81-48-467-4532; e-mail, sugita@riken.jp.

### Notes

The authors declare no competing financial interest.

## ■ ACKNOWLEDGMENTS

This research was supported in part by Grants-in-Aid for Young Scientists (B) of JSPS KAKENHI (Grant number: 23770192 to TM) and the Fund from the High Performance Computing Infrastructure (HPCI) Strategic Program of the Ministry of Education, Culture, Sports, Science and Technology (MEXT) (to YS). Some of the results were obtained on the K computer at the RIKEN Advanced Institute for Computational Science (Proposal number: hp120163 by TM and hp120309 by YS) and others using the RIKEN Integrated Cluster of Clusters (RICC) and the Fujitsu PRIMEHPC FX10 System (Oakleaf-FX) in the Information Technology Center, The University of Tokyo. TM gratefully acknowledges supports from the Special Postdoctoral Researchers Program of RIKEN.

## ■ REFERENCES

- (1) Gouaux, E.; MacKinnon, R. *Science* **2005**, *310*, 1461–1465.
- (2) Toyoshima, C. *Arch. Biochem. Biophys.* **2008**, *476*, 3–11.
- (3) White, S. H. *Nature* **2009**, *459*, 344–346.
- (4) Lee, A. G. *Biochim. Biophys. Acta* **2004**, *1666*, 62–87.
- (5) MacCallum, J. L.; Tielemans, D. P. *Trends Biochem. Sci.* **2011**, *36*, 653–662.
- (6) Mukherjee, S.; Maxfield, F. R. *Annu. Rev. Cell Dev. Biol.* **2004**, *20*, 839–866.
- (7) Lingwood, D.; Simons, K. *Science* **2010**, *327*, 46–50.
- (8) Service, R. F. *Science* **2013**, *339*, 264–266.

- (9) Shaw, D. E.; Deneroff, M. M.; Dror, R. O.; Kuskin, J. S.; Larson, R. H.; Salmon, J. K.; Young, C.; Batson, B.; Bowers, K. J.; Chao, J. C.; Eastwood, M. P.; Gagliardo, J.; Grossman, J. P.; Ho, C. R.; Ierardi, D. J.; Kolossváry, I.; Klepeis, J. L.; Layman, T.; McLeavey, C.; Moraes, M. A.; Mueller, R.; Priest, E. C.; Shan, Y. B.; Spengler, J.; Theobald, M.; Towles, B.; Wang, S. C. *Commun. ACM* **2008**, *51*, 91–97.
- (10) Dror, R. O.; Pan, A. C.; Arlow, D. H.; Borhani, D. W.; Maragakis, P.; Shan, Y. B.; Xu, H. F.; Shaw, D. E. *Proc. Natl. Acad. Sci. U. S. A.* **2011**, *108*, 13118–13123.
- (11) Jensen, M. Ø.; Jogini, V.; Borhani, D. W.; Leffler, A. E.; Dror, R. O.; Shaw, D. E. *Science* **2012**, *336*, 229–233.
- (12) Gumbart, J. C.; Teo, I.; Roux, B.; Schulten, K. *J. Am. Chem. Soc.* **2013**, *135*, 2291–2297.
- (13) Liwo, A.; Czaplewski, C.; Oldziej, S.; Scheraga, H. A. *Curr. Opin. Struct. Biol.* **2008**, *18*, 134–139.
- (14) Escobedo, F. A.; Borrero, E. E.; Araque, J. C. *J. Phys.: Condens. Mat.* **2009**, *21*, 333101.
- (15) Gullingsrud, J.; Schulten, K. *Biophys. J.* **2003**, *85*, 2087–2099.
- (16) Jensen, M. Ø.; Yin, Y.; Tajkhorshid, E.; Schulten, K. *Biophys. J.* **2007**, *93*, 92–102.
- (17) Cheng, X. L.; Wang, H. L.; Grant, B.; Sine, S. M.; McCammon, J. A. *PLoS Comput. Biol.* **2006**, *2*, 1173–1184.
- (18) Bond, P. J.; Holyoake, J.; Iveta, A.; Khalid, S.; Sansom, M. S. P. J. *Struct. Biol.* **2007**, *157*, 593–605.
- (19) Monticelli, L.; Kandasamy, S. K.; Periole, X.; Larson, R. G.; Tielemans, D. P.; Marrink, S. J. *J. Chem. Theory Comput.* **2008**, *4*, 819–834.
- (20) Yao, X. Q.; Kenzaki, H.; Murakami, S.; Takada, S. *Nat. Commun.* **2010**, *1*, 117.
- (21) Ohkubo, Y. Z.; Pogorelov, T. V.; Arcario, M. J.; Christensen, G. A.; Tajkhorshid, E. *Biophys. J.* **2012**, *102*, 2130–2139.
- (22) Berg, B. A.; Neuhaus, T. *Phys. Rev. Lett.* **1992**, *68*, 9–12.
- (23) Hansmann, U. H. E.; Okamoto, Y. *Phys. Rev. E* **1997**, *56*, 2228–2233.
- (24) Mitsutake, A.; Sugita, Y.; Okamoto, Y. *Biopolymers* **2001**, *60*, 96–123.
- (25) Itoh, S. G.; Okumura, H.; Okamoto, Y. *Mol. Simul.* **2007**, *33*, 47–56.
- (26) Sugita, Y.; Okamoto, Y. *Chem. Phys. Lett.* **1999**, *314*, 141–151.
- (27) Hukushima, K.; Nemoto, K. *J. Phys. Soc. Jpn.* **1996**, *65*, 1604–1608.
- (28) Okabe, T.; Kawata, M.; Okamoto, Y.; Mikami, M. *Chem. Phys. Lett.* **2001**, *335*, 435–439.
- (29) Paschek, D.; Garcia, A. E. *Phys. Rev. Lett.* **2004**, *93*, 238105.
- (30) Mori, Y.; Okamoto, Y. *J. Phys. Soc. Jpn.* **2010**, *79*, 074003.
- (31) Nagai, T.; Ueoka, R.; Okamoto, Y. *J. Phys. Soc. Jpn.* **2012**, *81*, 024002.
- (32) Vogel, A.; Roark, M.; Feller, S. E. *Biochim. Biophys. Acta* **2012**, *1818*, 219–224.
- (33) Nymeyer, H.; Woolf, T. B.; Garcia, A. E. *Proteins* **2005**, *59*, 783–790.
- (34) Kubo, H.; Okamoto, Y. *Chem. Phys. Lett.* **2004**, *383*, 397–402.
- (35) Im, W.; Brooks, C. L., III. *Proc. Natl. Acad. Sci. U. S. A.* **2005**, *102*, 6771–6776.
- (36) Miyashita, N.; Straub, J. E.; Thirumalai, D.; Sugita, Y. *J. Am. Chem. Soc.* **2009**, *131*, 3438–3439.
- (37) Sayadi, M.; Tanizaki, S.; Feig, M. *Biophys. J.* **2010**, *98*, 805–814.
- (38) Zhang, Y. H.; Feller, S. E.; Brooks, B. R.; Pastor, R. W. *J. Chem. Phys.* **1995**, *103*, 10252–10266.
- (39) Israelachvili, J. N.; Mitchell, D. J.; Ninham, B. W. *Biochim. Biophys. Acta* **1977**, *470*, 185–201.
- (40) Jähnig, F. *Biophys. J.* **1996**, *71*, 1348–1349.
- (41) Butler, P. J.; Tsou, T. C.; Li, J. Y. S.; Usami, S.; Chien, S. *FASEB J.* **2001**, *15*, 216–218.
- (42) Butler, P. J.; Norwich, G.; Weinbaum, S.; Chien, S. *Am. J. Physiol.-Cell Physiol.* **2001**, *280*, C962–C969.
- (43) Nagle, J. F.; Tristram-Nagle, S. *Biochim. Biophys. Acta* **2000**, *1469*, 159–195.
- (44) Mori, Y.; Okamoto, Y. *J. Phys. Soc. Jpn.* **2010**, *79*, 074001.

- (45) Martyna, G. J.; Tobias, D. J.; Klein, M. L. *J. Chem. Phys.* **1994**, *101*, 4177–4189.
- (46) Feller, S. E.; Zhang, Y. H.; Pastor, R. W.; Brooks, B. R. *J. Chem. Phys.* **1995**, *103*, 4613–4621.
- (47) Quigley, D.; Probert, M. I. *J. Chem. Phys.* **2004**, *120*, 11432–11441.
- (48) Ferrenberg, A. M.; Swendsen, R. H. *Phys. Rev. Lett.* **1988**, *61*, 2635–2638.
- (49) Kumar, S.; Bouzida, D.; Swendsen, R. H.; Kollman, P. A.; Rosenberg, J. M. *J. Comput. Chem.* **1992**, *13*, 1011–1021.
- (50) Jo, S.; Kim, T.; Im, W. *PLoS One* **2007**, *2*, e880.
- (51) Klauda, J. B.; Venable, R. M.; Freites, J. A.; O'Connor, J. W.; Tobias, D. J.; Mondragon-Ramirez, C.; Vorobyov, I.; MacKerell, A. D., Jr.; Pastor, R. W. *J. Phys. Chem. B* **2010**, *114*, 7830–7843.
- (52) Brünger, A.; Brooks, C. L., III; Karplus, M. *Chem. Phys. Lett.* **1984**, *105*, 495–500.
- (53) Loncharich, R. J.; Brooks, B. R.; Pastor, R. W. *Biopolymers* **1992**, *32*, 523–535.
- (54) Ryckaert, J. P.; Ciccotti, G.; Berendsen, H. J. C. *J. Comput. Phys.* **1977**, *23*, 327–341.
- (55) Miyamoto, S.; Kollman, P. A. *J. Comput. Chem.* **1992**, *13*, 952–962.
- (56) Essmann, U.; Perera, L.; Berkowitz, M. L.; Darden, T.; Lee, H.; Pedersen, L. G. *J. Chem. Phys.* **1995**, *103*, 8577–8593.
- (57) Jung, J.; Mori, T.; Sugita, Y. *J. Comput. Chem.* **2013**, *34*, 2412–2420.
- (58) Jung, J.; Mori, T.; Kobayashi, C.; Imai, T.; Yoda, T.; Matsunaga, Y.; Galvelis, R.; Nishima, W.; Harada, R.; Miyashita, N.; Karino, Y.; Sugita, Y. Manuscript in preparation.
- (59) Weiss, T. M.; van der Wel, P. C. A.; Killian, J. A.; Koepppe, R. E.; Huang, H. W. *Biophys. J.* **2003**, *84*, 379–385.
- (60) MacKerell, A. D., Jr.; Bashford, D.; Bellott, M.; Dunbrack, R. L., Jr.; Evanseck, J. D.; Field, M. J.; Fischer, S.; Gao, J.; Guo, H.; Ha, S.; Joseph-McCarthy, D.; Kuchnir, L.; Kuczera, K.; Lau, F. T. K.; Mattos, C.; Michnick, S.; Ngo, T.; Nguyen, D. T.; Prodhom, B.; Reiher, W. E., III; Roux, B.; Schlenkrich, M.; Smith, J. C.; Stote, R.; Straub, J.; Watanabe, M.; Wiórkiewicz-Kuczera, J.; Yin, D.; Karplus, M. *J. Phys. Chem. B* **1998**, *102*, 3586–3616.
- (61) MacKerell, A. D., Jr.; Feig, M.; Brooks, C. L., III. *J. Comput. Chem.* **2004**, *25*, 1400–1415.
- (62) Shinoda, W.; Okazaki, S. *J. Chem. Phys.* **1998**, *109*, 1517–1521.
- (63) Mori, T.; Ogushi, F.; Sugita, Y. *J. Comput. Chem.* **2012**, *33*, 286–293.
- (64) Klauda, J. B.; Brooks, B. R.; Pastor, R. W. *J. Chem. Phys.* **2006**, *125*, 144710.
- (65) Sheats, J. R.; McConnell, H. M. *Proc. Natl. Acad. Sci. U. S. A.* **1978**, *75*, 4661–4663.
- (66) Anežo, C.; de Vries, A. H.; Höltje, H. D.; Tielemans, D. P.; Marrink, S. J. *J. Phys. Chem. B* **2003**, *107*, 9424–9433.
- (67) Galla, H. J.; Hartmann, W.; Theilen, U.; Sackmann, E. *J. Membr. Biol.* **1979**, *48*, 215–236.
- (68) Muddana, H. S.; Gullapalli, R. R.; Manias, E.; Butler, P. J. *Phys. Chem. Chem. Phys.* **2011**, *13*, 1368–1378.
- (69) Reddy, A. S.; Warshavskiak, D. T.; Chachisvilis, M. *Biochim. Biophys. Acta* **2012**, *1818*, 2271–2281.
- (70) Klauda, J. B.; Roberts, M. F.; Redfield, A. G.; Brooks, B. R.; Pastor, R. W. *Biophys. J.* **2008**, *94*, 3074–3083.
- (71) Kim, T.; Im, W. *Biophys. J.* **2010**, *99*, 175–183.
- (72) Wang, Y.; Markwick, P. R. L.; de Oliveira, C. A. F.; McCammon, J. A. *J. Chem. Theory Comput.* **2011**, *7*, 3199–3207.
- (73) Sulkharev, S.; Betanzos, M.; Chiang, C. S.; Guy, H. R. *Nature* **2001**, *409*, 720–724.
- (74) Tsukazaki, T.; Mori, H.; Fukai, S.; Ishitani, R.; Mori, T.; Dohmae, N.; Perederina, A.; Sugita, Y.; Vassilyev, D. G.; Ito, K.; Nureki, O. *Nature* **2008**, *455*, 988–992.
- (75) Mori, T.; Ishitani, R.; Tsukazaki, T.; Nureki, O.; Sugita, Y. *Biochemistry* **2010**, *49*, 945–950.
- (76) Ikeguchi, M. *J. Comput. Chem.* **2004**, *25*, 529–541.